

Observation of persistent centrosymmetry in the hexagonal manganite family

Yu Kumagai,^{1,*} Alexei A. Belik,² Martin Lilienblum,¹ Naëmi Leo,¹ Manfred Fiebig,¹ and Nicola A. Spaldin¹

¹Department of Materials, ETH Zurich, Wolfgang-Pauli-Strasse 10, 8093 Zurich, Switzerland

²International Center for Materials Nanoarchitectonics (WPI-MANA), NIMS, Namiki 1-1, Ibaraki 305-0044, Japan

(Dated: October 26, 2018)

The controversy regarding the ferroelectric behavior of hexagonal InMnO_3 is resolved by using a combination of x-ray diffraction (XRD), piezoresponse force microscopy (PFM), second harmonic generation (SHG), and density functional theory (DFT). While XRD data show a symmetry-lowering unit-cell tripling, which is also found in the multiferroic hexagonal manganites of $P6_3cm$ symmetry, PFM and SHG do not detect ferroelectricity at ambient or low temperature, in striking contrast to the behavior in the multiferroic counterparts. We propose instead a centrosymmetric $P\bar{3}c$ phase as the ground state structure. Our DFT calculations reveal that the relative energy of the ferroelectric and nonferroelectric structures is determined by a competition between electrostatics and oxygen- R -site covalency, with an *absence* of covalency favoring the ferroelectric phase.

I. INTRODUCTION: STRUCTURE OF THE HEXAGONAL MANGANITES

Hexagonal h-RMnO_3 ($R = \text{Sc, Y, Dy-Lu}$) represents an established class of multiferroics in which ferroelectricity and antiferromagnetism exist simultaneously. Although their fundamental properties have been investigated for half a century, recent reports of intriguing characteristics such as interlocked antiphase (AP) and ferroelectric (FE) (AP+FE) domain walls¹⁻³ are fueling continued interest. At the root of these behaviors is their unusual improper geometric ferroelectricity,^{4,5} which is in turn related to their layered structure, in which xy planes of R^{3+} ions are interspaced by layers of corner-shared MnO_5 trigonal polyhedra (Fig. 1).

InMnO_3 crystallizes in the same hexagonal manganite structure as the h-RMnO_3 compounds, and might be expected to show analogous ferroelectric behavior. In fact, most previous x-ray and neutron powder diffraction refinements assigned InMnO_3 to the polar $P6_3cm$ structure adopted by the multiferroic hexagonal manganites.⁶⁻⁸ In the $P6_3cm$ structure, the MnO_5 trigonal bipyramids tilt and trimerize with a trimerization phase of $n \cdot 60^\circ$, where n is an integer. The R ions on the $2a$ sites displace up or down along the z direction, depending on the tilting direction, and those on the $4b$ sites in the opposite direction (Fig. 1). This tilt symmetry then enables an additional displacement of the R sublattice relative to the Mn-O layers causing a net ferroelectric polarization. Rusakov and Belik *et al.* pointed out that the nonpolar $P\bar{3}c$ structure – in which the MnO_5 polyhedra trimerize at intermediate angles and the inversion symmetry is retained (Fig. 1) – and polar $P6_3cm$ structure have similar powder x-ray-diffraction R values.⁹ They disregarded the $P\bar{3}c$ model in their subsequent analysis, however, believing that all h-RMnO_3 compounds should be polar. Indeed, ferroelectricity has been reported in InMnO_3 below 500 K based on the observation of polarization-electric field (P-E) hysteresis loops obtained by a ferroelectric test system. Such pyroelectric current measurements, especially if they are applied to amorphous samples or thin films, are notoriously sensitive to sample defects, however, and the P-E loops shown in Ref. 10 could indicate leaky dielectric behavior rather than ferroelectricity.¹¹ In agreement with this, Belik *et al.* did not observe spontaneous polariza-

tion when they repeated the experiment.^{7,9} Therefore there is no clear evidence to date that InMnO_3 has the $P6_3cm$ structure or shows ferroelectric polarization.

In this study, we revisit the structure and polarization behavior of InMnO_3 by using a combination of x-ray diffraction (XRD), piezoresponse force microscopy (PFM), optical second harmonic generation (SHG), and density functional theory (DFT) and show that InMnO_3 is indeed centrosymmetric, with $P\bar{3}c$ as the most likely space group (Fig. 1). We explain the difference between InMnO_3 and the multiferroic h-RMnO_3 compounds using DFT analysis of the chemical bonding, and propose another candidate material TiMnO_3 that should also show the nonferroelectric InMnO_3 structure. Finally, we discuss the implications of this newly-identified structure for the multiferroicity in the h-RMnO_3 family in general.

II. EXPERIMENTS

A. XRD

First we use powder XRD to directly and quantitatively compare the refinements for the candidate polar and nonpolar structures. For sample preparation, a stoichiometric mixture of In_2O_3 (99.9%) and Mn_2O_3 was placed in Au capsules and treated at 6 GPa in a belt-type high pressure apparatus at 1373 K for 30 min (heating rate 110 K/min). After heat treatment, the samples were quenched to room temperature, and the pressure was slowly released. The resultant samples were black dense pellets. Single-phase Mn_2O_3 was prepared from commercial MnO_2 (99.99%) by heating in air at 923 K for 24 h. The synchrotron XRD data were obtained on powdered samples at the BL02B2 beamline of SPring-8.¹² They were collected in a 2θ range from 2° to 75° with a step interval of 0.01 degrees and analyzed by the Rietveld method with RIETAN-2000.¹³

An evaluation of the XRD data shown in Fig. 2 clearly reveals that the unit cell of InMnO_3 holds six formula units. This indicates a deviation of the $P6_3/mmc$ high-temperature phase due to unit-cell tripling with tilt-shear motions of the MnO_5 bipyramids as in the ferroelectric RMnO_3 compounds.

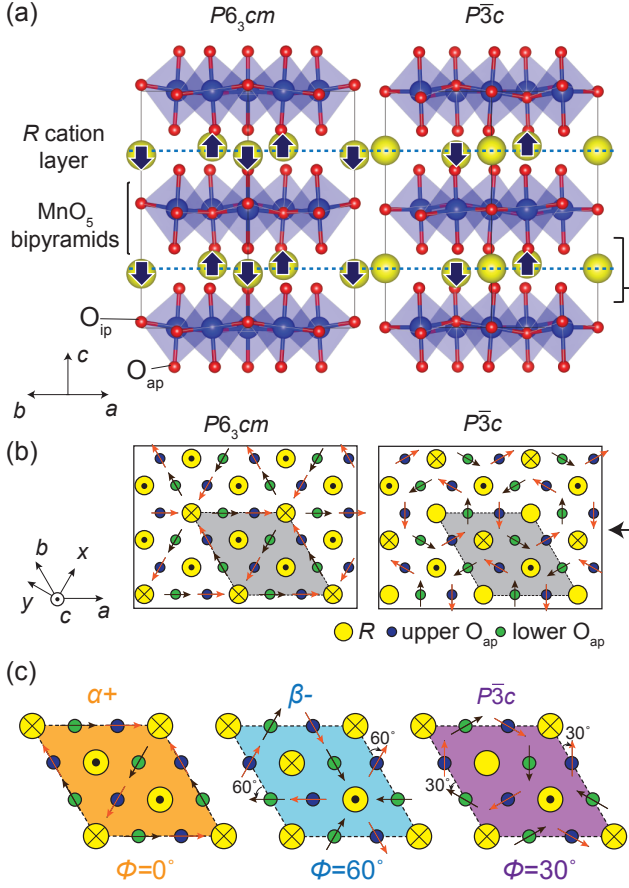


FIG. 1: (a) Side and (b) top views of the two candidate $InMnO_3$ structures. $P6_3cm$ is the ferroelectric phase of the $h-RMnO_3$ compounds; $P\bar{3}c$ is the structure proposed for $InMnO_3$ in this study. Arrows indicate the displacements from the high symmetry $P6_3/mmc$ phase. The primitive unit cell is shaded grey. In contrast with the $P6_3cm$ phase, one In ion in the $P\bar{3}c$ unit cell remains at the high-symmetry $2b$ site, retaining the inversion symmetry. Note also the different tilt patterns of the MnO_5 polyhedra toward or around corner R ions. (c) Top views of α^+ and β^- domains in the $P6_3cm$ phase using the notation from Ref. 1 and one of six domains in the $P\bar{3}c$ phase. The phases Φ , defined by the (counter)clockwise angle of tilting direction of upper (lower) oxygen layers relative to α^+ domain, are also shown (Ref. 1). Note that the $P\bar{3}c$ phase has a tilt phase of $30^\circ + n \cdot 60^\circ$, and is obtained by averaging the tilt patterns and R -ion displacements of two $P6_3cm$ trimerization domains with different origins and orientations such as the α^+ and β^- domains.

The centrosymmetric and the noncentrosymmetric subgroups with the highest possible symmetry that are compatible with a trimerization of the $P6_3/mmc$ high-temperature phase are $P6_3/mcm$ and $P6_3cm$, respectively. Here refinements clearly favor the latter structure which may contribute to former claims of the $P6_3cm$ symmetry for $InMnO_3$.⁹ However, in contrast to the case of the ferroelectric manganites, the structure refinements of the XRD data reveals equally good fits for the centrosymmetric space group $P\bar{3}c$ and the noncentrosymmetric space group $P6_3cm$ ¹⁴ consistent with a previous observation.⁹ In Table I we report our refined atomic co-

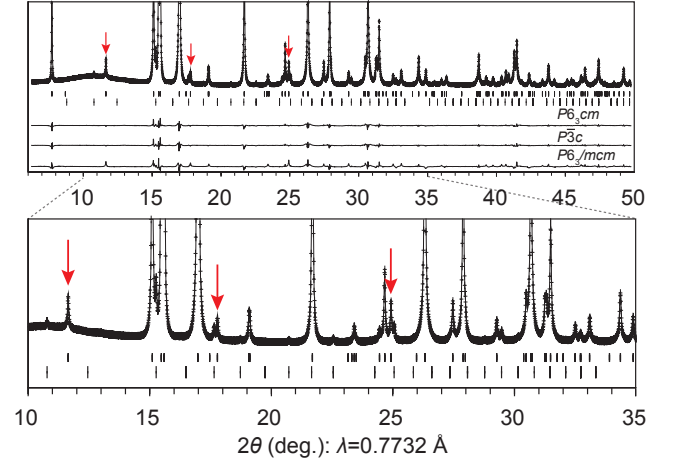


FIG. 2: Synchrotron x-ray powder diffraction patterns of $InMnO_3$ at 293 K. Crosses represent data points and solid lines calculated intensities for $P\bar{3}c$. Differences for three structure models are also shown. Bragg reflections are indicated by tick marks (these are the same for $P6_3cm$, $P\bar{3}c$, and $P6_3/mcm$ models). The lower tick marks indicate reflections from In_2O_3 impurity. Arrows show reflections corresponding to unit-cell tripling.

TABLE I: Atomic fractional coordinates for $InMnO_3$ at 293 K in space group $P\bar{3}c$ (top) and $P6_3cm$ (bottom), obtained in this work using powder XRD. Our measured lattice constants a and c are 5.88462(10) and 11.48540(15) Å for $P\bar{3}c$ and 5.88463(7) and 11.48541(12) Å for $P6_3cm$, respectively.

$P\bar{3}c$					
Atom	Wyckoff position	x	y	z	B_{iso} (Å ²)
In1	4d	1/3	2/3	0.51674(8)	0.46(3)
In2	2b	0	0	0	1.28(8)
Mn	6f	0.6587(10)	0	1/4	0.36(2)
O1	2a	0	0	1/4	0.9(4)
O2	4d	1/3	2/3	0.7312(7)	0.26(15)
O3	12g	0.6829(25)	0.0241(10)	0.0858(2)	0.77(8)

$P6_3cm$					
Atom	Wyckoff position	x	y	z	B_{iso} (Å ²)
In1	2a	0	0	0.2674(6)	0.33(6)
In2	4b	1/3	2/3	0.2383(6)	0.92(4)
Mn	6c	0.3250(10)	0	0	0.37(3)
O1	6c	0.3117(22)	0	0.1749(11)	1.5(3)
O2	6c	0.6466(18)	0	0.3445(10)	-0.4(2)
O3	2a	0	0	0.4746(20)	-0.2(4)
O4	4b	1/3	2/3	0.0077(20)	0.7(3)

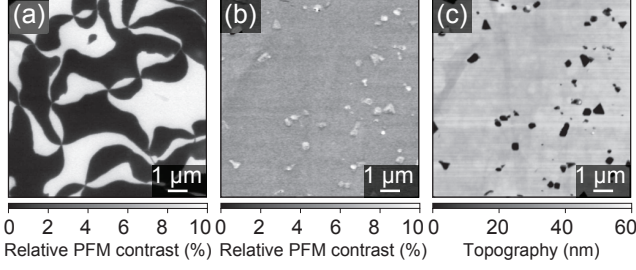


FIG. 3: PFM images scaled relative to the response of periodically poled lithium niobate at room temperature, for (a) YMnO_3 showing the known characteristic ferroelectric domain pattern, and for (b) InMnO_3 , where no ferroelectric domains are observed, and only topographical artifacts (c) are visible.

ordinates and lattice parameters within the $P\bar{3}c$ and $P6_3cm$ space groups. In general, structures refined with the correct space group are lower in energy than those refined with incorrect space groups. Our DFT calculations for InMnO_3 at the atomic positions and cell parameters obtained in the two competing best-fit experimental refinements (calculation details given later) indicate that the nonpolar $P\bar{3}c$ structure is ~ 200 meV per formula unit (f.u.) lower in energy than the $P6_3cm$ structure. We therefore suggest the nonferroelectric $P\bar{3}c$ phase as the ground state for InMnO_3 .

B. PFM

To confirm this suggestion, we next used PFM to probe directly for the presence of FE domains; this technique avoids ambiguities caused by sample leakiness which might have occurred in previous macroscopic polarization measurements.¹⁰ In order to calibrate the response from InMnO_3 , PFM and simultaneous scanning force microscopy (SFM) measurements with a commercial SFM (Solaris, NT-MDT) were carried out on YMnO_3 and InMnO_3 . All compounds for PFM and SHG measurements were grown by the flux method as z -oriented platelets.¹⁵ For PFM an ac-voltage of 14 V_{pp} at a frequency of 40 kHz was applied to a conductive Pt-Ir coated probe (NSC 35, Mikromasch). The out-of-plane component of the piezoelectric response was recorded by the in-phase output channel of an external lock-in amplifier (SR830, Stanford Research) with a typical sensitivity of 200 μV and time constant of 10 ms. The PFM signal of each sample was normalized to a response of the z face of PPLN ($d_{33}=7$ pm/V) in order to maintain comparability of the PFM response, which was measured before and after each h- RMnO_3 measurement in order to exclude changes in the PFM sensitivity.¹⁶

Our results are summarized in the equally scaled Figs. 3(a) and 3(b). YMnO_3 reveals the familiar domain pattern of six intersecting AP+FE domains with alternating polarization $\pm P_z$.^{1,2} Strikingly, the InMnO_3 shows an almost homogeneous distribution of the PFM response with no sign of FE domains. The corresponding SFM data in Fig. 3(c) show that the slightly brighter speckles in the PFM image correspond to

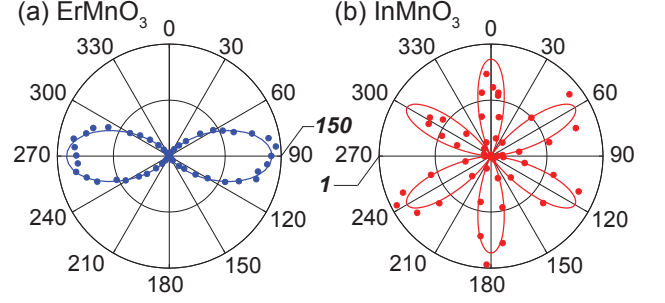


FIG. 4: SHG on (a) ErMnO_3 and (b) InMnO_3 at 5 K and 2.51 eV with light incident on the z -oriented surface of the single crystals along the $[011]$ direction. The anisotropy measurement was obtained by rotating the linear polarization of the incident light at ω and of the detected intensity at 2ω simultaneously by 360° . Lines are fits of the SHG data according to Ref. 18. Scales in (a) and (b) differ by a factor 150. The two-fold SHG signal of ErMnO_3 indicates the presence of a spontaneous polarization whereas no indication for ferroelectricity in InMnO_3 was found. Instead the six-fold pattern characteristic of the antiferromagnetic order in InMnO_3 is observed.

protrusions on the unpolished surface of the InMnO_3 sample. If one relates the contrast obtained for opposite domains in YMnO_3 to the spontaneous polarization of $5.6 \mu\text{C}/\text{cm}^2$, any polarization in InMnO_3 has to be at least two orders of magnitude smaller to avoid detection in our measurement. Our calculated polarization¹⁷ for the DFT-optimized $P6_3cm$ InMnO_3 structure is $4.8 \mu\text{C}/\text{cm}^2$ which would certainly be detectable. The absence of ferroelectricity (or of sub-resolution domains) in InMnO_3 is further supported by poling experiments with the SFM tip which did not induce any lasting change of the PFM response.

C. SHG

Since PFM measurements could only be done under ambient conditions, we next used SHG to search for ferroelectric order at low temperature. As discussed in detail in Ref. 19, the breaking of inversion symmetry by ferroelectric order leads to a characteristic SHG signal. The samples were mounted in a liquid-helium-operated cryostat and probed with 120 fs laser pulses in a standard transmission setup for SHG.¹⁹ For comparison, ErMnO_3 was chosen for the SHG data because, unlike YMnO_3 , it has the same magnetic SHG spectrum as InMnO_3 . Figure 4 shows the anisotropy of the SHG signal taken under identical conditions at 5 K on ferroelectric ErMnO_3 and on InMnO_3 . The laser light was incident under 45° to the hexagonal crystal axes so that SHG components coupling to a spontaneous polarization along z could be excited.¹⁹ ErMnO_3 shows the double lobe characteristic of the ferroelectric order. In InMnO_3 the double lobe is absent. Instead a SHG signal with the sixfold anisotropy characteristic of the antiferromagnetic order and 150 times weaker intensity is found, indicating that the only order parameter is the antiferromagnetism of the Mn^{3+} ions. We therefore conclude that

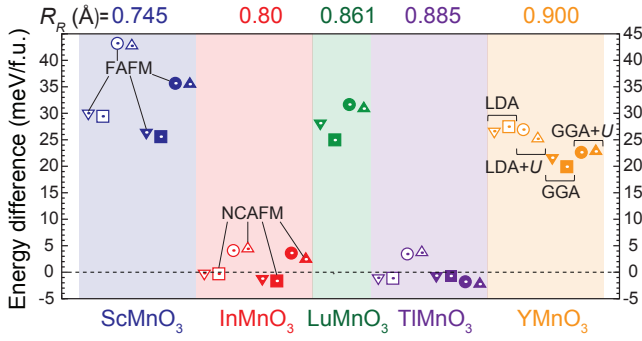


FIG. 5: Calculated energy differences between the fully relaxed $P\bar{3}c$ phase and $P6_3cm$ phases, ΔE_{str} . Four exchange-correlation functionals, LDA, GGA, LDA+U, and GGA+U, and two spin configurations, FAFM and NCAFM (see text), were used. LDA/LDA+U results for LuMnO₃ are not shown because VASP does not provide an LDA Lu PAW potential. Positive ΔE_{str} indicates that the ferroelectric $P6_3cm$ phase is stable over the $P\bar{3}c$ phase. The compounds are plotted in order of increasing R -site cation ionic radii, R_R (Ref. 20).

InMnO₃ is not ferroelectric down to 5 K.

III. THEORY

To resolve the origin of the difference between InMnO₃ and the other hexagonal manganite h-RMnO₃ compounds, we used DFT calculations to evaluate the energy difference, $\Delta E_{\text{str}} = E_{P\bar{3}c} - E_{P6_3cm}$, between the candidate $P6_3cm$ and $P\bar{3}c$ phases. Our spin-polarized first principles calculations were performed using the projector augmented-wave (PAW) method²¹ as implemented in VASP.²² In this study, Sc 3s, 3p, 3d, and 4s, Y 4s, 4p, 4d, and 5s, In 5s and 5p, Lu 5p, 5d, and 6s, Tl 6s and 6p, Mn 3d and 4s, and O 2s and 2p were described as valence electrons. The PAW data set with radial cutoffs of 1.3, 1.4, 1.6, 1.6, 1.7, 1.2, and 0.8 Å, respectively, for Sc, Y, In, Lu, Tl, Mn and O was employed. The local density of states was also evaluated within the same spheres. Wave functions were expanded with plane waves up to an energy cutoff of 500 eV. All calculations were performed with 30-atom cells, which can describe unit cells of $P6_3cm$ and $P\bar{3}c$ phases. k -points were sampled with a Γ -centered $4 \times 4 \times 2$ grid. In addition to InMnO₃, we also calculated ΔE_{str} for ScMnO₃, LuMnO₃, and YMnO₃, as well as for as-yet-unsynthesized TiMnO₃. To validate the results, we adopted four different exchange-correlation (XC) functionals: local density approximation (LDA), generalized gradient approximation (GGA), LDA+U, and GGA+U,^{23–25} with the value for $U_{\text{eff}} = U - J$ on the Mn-3d orbitals set to 4 eV. In addition we tested two different spin configurations, so-called frustrated antiferromagnetic (FAFM)²⁶ and the noncollinear antiferromagnetic (NCAFM) adopted in Ref. 27. The lattice constants and internal positions were fully optimized in each case until the residual stresses and forces converged to less than 0.1 GPa and 0.01 eV/Å respectively.

Figure 5 shows our calculated ΔE_{str} values for the various

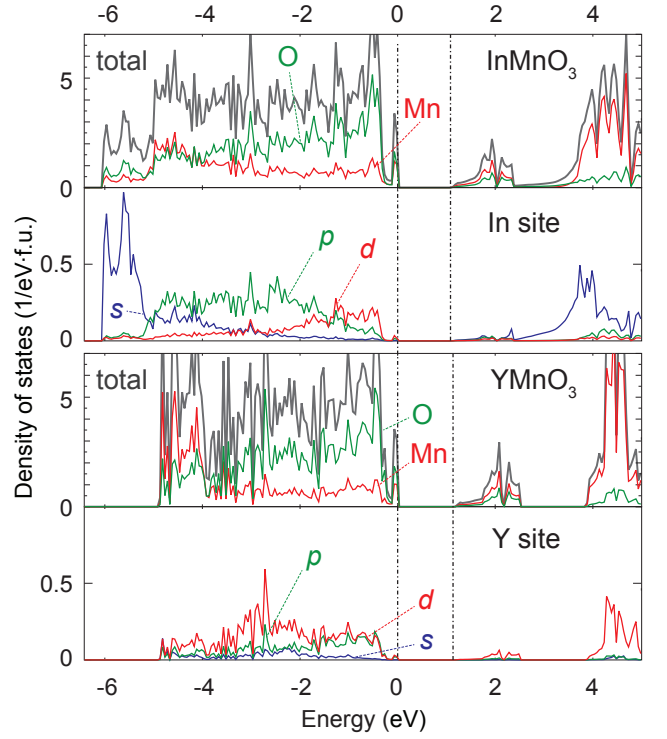


FIG. 6: Calculated total and averaged local densities of states for InMnO₃ and YMnO₃ in the $P\bar{3}c$ phase. Zeroes of the horizontal axes are set to the top of the valence band. Valence bands are composed mainly of O-2p and Mn-3d orbitals. The difference of the electronic structures is mainly manifested at the formally unoccupied R 5s and 5p local density of states.

functionals and magnetic configurations. A positive ΔE_{str} indicates that the ferroelectric structure is stable. When the R site is occupied with a IIIb (Sc, Y, or Lu) ion, the $P6_3cm$ phase is more stable than the $P\bar{3}c$ phase consistent with the experimentally observed ferroelectricity. However, in the case of a IIIa (In or Tl) ion, ΔE_{str} is close to zero. Note that in these calculations the lattice parameters and ionic positions for both structures were fully relaxed, within the constraint of the appropriate symmetry. [When we previously constrained our atomic positions and cell parameters to those obtained from the XRD analysis, the energy of the $P\bar{3}c$ phase is much lower (~ 200 meV/f.u.) than that of the $P6_3cm$ phase as we reported in Sec. II A.] We note that ΔE_{str} is quite insensitive to the magnetic configuration, but does show a dependence on the choice of XC functional, and for InMnO₃, the sign of ΔE_{str} depends on the functional, suggesting the possibility of competing low energy structures.²⁸ [Previous calculations of the energy difference between $P6_3cm$ and $P\bar{3}c$ structures for InMnO₃ derived from XRD data (Sec. II A) and the polarization for InMnO₃ with the $P6_3cm$ symmetry (Sec. II B), and subsequent calculations use the GGA+U and FAFM configuration.]

It is clear from Fig. 5 that R_R is not the key factor in determining the phase stability. Instead we focus on the different chemistry of the group IIIa ions, compared to the group

IIIb ions. It was previously suggested that the behavior of InMnO_3 is dominated by high-lying occupied semicore $4d$ (In) electrons;²⁷ in contrast the valence d states are formally unoccupied in the IIIb ions. In fact it is well known that the presence or absence of semicore d electrons can affect the structural stability as illustrated by the different structures of MgO (rock salt) and ZnO (wurtzite, with semicore ds) in which the cations have very similar ionic radii ($r_{\text{MgO}} = 0.57 \text{ \AA}$ and $r_{\text{ZnO}} = 0.60 \text{ \AA}$ in four-coordination and $r_{\text{MgO}} = 0.72 \text{ \AA}$ and $r_{\text{ZnO}} = 0.74 \text{ \AA}$ in six-coordination).

In Fig. 6(a) we show our calculated densities of states (DOS) for InMnO_3 and YMnO_3 (TiMnO_3 , and $\text{ScMnO}_3/\text{LuMnO}_3$ behave analogously to InMnO_3 and YMnO_3 , respectively), both calculated within the $P\bar{3}c$ phase to allow a direct comparison. In both cases, the valence bands consist mainly of Mn- d (up-spin e_{1g} and e_{2g}) and O- $2p$ states. The main differences occur in the DOSs on the R ions. The In “semicore” $4d$ states, however, form a narrow band that is around -13 eV below the top of the valence band when the d electrons are treated as valence (not shown). They do not directly contribute to covalent bonding with the oxygen anions, in contrast to the suggestion in Ref. 27. The relevant difference is the substantially lower energy of the formally unoccupied R $5s$ and $5p$ states in In compared with Y, caused by the well-known increase in nuclear charge without corresponding increase in screening across the $4d$ series. As a result, in InMnO_3 the $5s$ (and to a lesser extent $5p$) states, which would be completely empty in the ionic limit, develop significant occupation through In-O $2p$ covalency, with occupied In $5s$ states in fact forming the bottom of the valence band. (Similar behavior has been previously reported in other In oxides.^{29,30}) In YMnO_3 , the Y $5s$ and $5p$ states are substantially higher in energy relative to the top of the valence band and so their hybridization with O $2p$ and subsequent occupation is negligible. Instead there is a small hybridization with the formally empty Y $4d$ states.

The difference in covalency between InMnO_3 and YMnO_3 manifests particularly strikingly in the calculated valence charge densities at the R sites. In Fig. 7 we show the valence charge density differences between LuMnO_3 and YMnO_3 and between InMnO_3 and YMnO_3 in the $P\bar{3}c$ structure. The charge density at the Mn sites is similar in all cases. Compared with YMnO_3 and LuMnO_3 , however, InMnO_3 has a decrease in charge density at the O sites adjacent to the In ions and an increase at the outer region of the In site indicating charge transfer from oxygen to In and stronger In-O than Y-O or Lu-O covalent bond formation.

Next we investigate how the additional covalency of the In-O and Ti-O bonds compared with those of Y-O and related compounds manifest in the spring constants. Our calculated z -direction spring constants of the R ions at the high-symmetry $2b$ sites in the $P\bar{3}c$ structure are 2.7 , 3.2 , and 3.1 eV/\AA^2 for ScMnO_3 , LuMnO_3 , and YMnO_3 , and are 4.4 and 4.2 eV/\AA^2 for InMnO_3 and TiMnO_3 . As expected, the strong In-O and Ti-O hybridization results in larger spring constants in the In and Ti compounds. The larger spring constants make the In and Ti ions reluctant to shift from their high-symmetry sites, favoring instead equal $R\text{-O}_{\text{ap}}$ bond distances. This in turn fa-

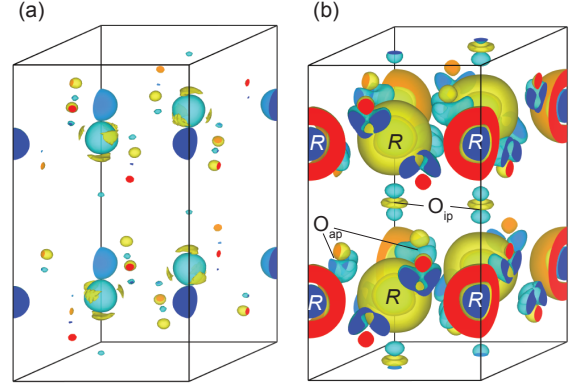


FIG. 7: Charge density differences for valence band electrons between (a) LuMnO_3 and YMnO_3 and (b) InMnO_3 and YMnO_3 in the $P\bar{3}c$ phase. For the comparison, the same atomic positions were chosen for the compounds that are compared. The structures are constructed by averaging the DFT-optimized structures for (a) LuMnO_3 and YMnO_3 , and (b) InMnO_3 and YMnO_3 . Red and blue regions correspond to excess and deficiency of charge in $\text{LuMnO}_3/\text{InMnO}_3$ compared with YMnO_3 . The yellow and light blue isosurfaces correspond to 0.03 and -0.03 \AA^{-3} , respectively. Comparing with the charge density difference between LuMnO_3 and YMnO_3 , InMnO_3 shows noticeable differences from YMnO_3 especially at the In site.

vors the $P\bar{3}c$ structure, in which $\frac{1}{3}$ of the R ions retain their fully 6-coordinated high-symmetry positions, over the ferroelectric $P6_3cm$ phase, in which all R ions are displaced from the high-symmetry positions.

We emphasize that the behavior here in which stronger covalency favors the nonferroelectric phase is completely different from that in conventional ferroelectrics such as BaTiO_3 , in which stronger covalency favors the ferroelectric distortion through the second-order Jahn-Teller effect. In such conventional ferroelectrics, the Born effective charges $Z^* = \frac{\partial P}{\partial u}$ which participate actively in the re-hybridization are anomalously larger than the formal ionic charges, reflecting the charge transfer that takes place during the ionic displacements to the ferroelectric phase; such anomalous Born effective charges are signatures of instability toward a ferroelectric phase transition.³¹ In both InMnO_3 and YMnO_3 the mechanism for the primary symmetry-lowering tilt distortion is geometric rather than due to a rehybridization, and the Born effective charges on all atoms are nonanomalous.³² In InMnO_3 , the additional strong In-O covalency in the paraelectric phase resists the distortion of the In ions away from their high-symmetry positions favoring the $P\bar{3}c$ space group, whereas the lower Y-O covalency provides less resistance, allowing the additional Y-O displacements required to reach the $P6_3cm$ symmetry. In Ref. 33, the hybridization between the Y- $3d$ and O- $2p$ orbitals was measured using polarization-dependent x-ray absorption spectroscopy (XAS) at the O K -edge. Then the static charge occupancy in the Y $3d$ orbitals was equated with an anomalous dynamical Born effective charge, which led to the claim that this hybridization is responsible for the ferroelectricity in YMnO_3 . It is important to understand that the Born effective charge is the derivative of the polarization with

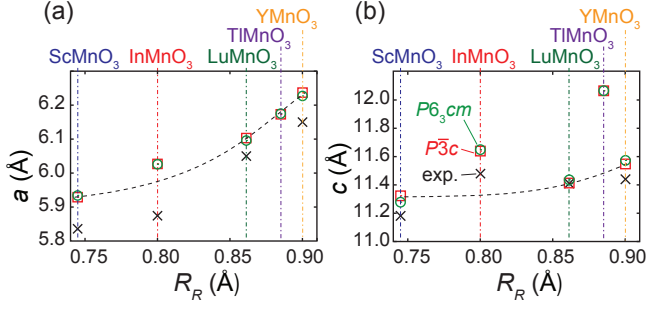


FIG. 8: Calculated (a) in-plane and (b) out-of-plane lattice constants in the $P6_3cm$ (\circ) and $P\bar{3}c$ (\square) phases. The experimental lattice constants are also shown (\times) (Ref. 6,34,35). The dashed lines indicate the trend of IIIb manganites for a guide to eyes.

respect to ionic displacements, and is unrelated to the static orbital occupancy in a single structure: Partial hybridization of Y 3d with O 2p, while clearly present both in the experiments and in earlier and subsequent first-principles calculations, is not indicative of an anomalous Born effective charge and therefore does not indicate tendency toward ferroelectricity.

Experimentally, it is known that InMnO_3 has an anomalously large c lattice constant compared to the multiferroic hexagonal manganites.⁶ In Fig. 8 we plot our calculated lattice constants (with experimental values where available for comparison) of the manganites series as a function of ionic radii R_R . We point out first that this is not a consequence of the different space group that we have established here; our density functional calculations yield similar lattice constants for InMnO_3 in the $P\bar{3}c$ and $P6_3cm$ phases. The calculated lattice constants are systematically overestimated compared with experiments as is typical of the GGA. We see that the in-plane lattice constants, a , increase monotonically with R_R , with InMnO_3 showing only a small calculated anomaly. In contrast, the c lattice constant of InMnO_3 deviates strongly from the trend shown by the IIIb manganites, both in our calculations and in experiment. Since this deviation is also identified in TiMnO_3 , the anomalously large c likely originates from covalency in IIIa manganites as shown in Fig. 7.

IV. DISCUSSION

Although the centrosymmetric $P\bar{3}c$ phase that we propose in this work for InMnO_3 may be seemingly less attractive compared with the ferroelectric $P6_3cm$ structure, our results have implications for the multiferroic hexagonal manganites as a whole. Since the tilt pattern of the YMnO_3 structure subsequently allows for the development of ferroelectricity, whereas that of the InMnO_3 structure does not, the subtle chemical bonding differences identified here that favor one tilt pattern over another in turn determine whether the resulting structure can be multiferroic. Specifically, we have discussed here that an *absence* of R -O hybridization is required to favor the YMnO_3 tilt pattern over the InMnO_3 tilt pattern; an ab-

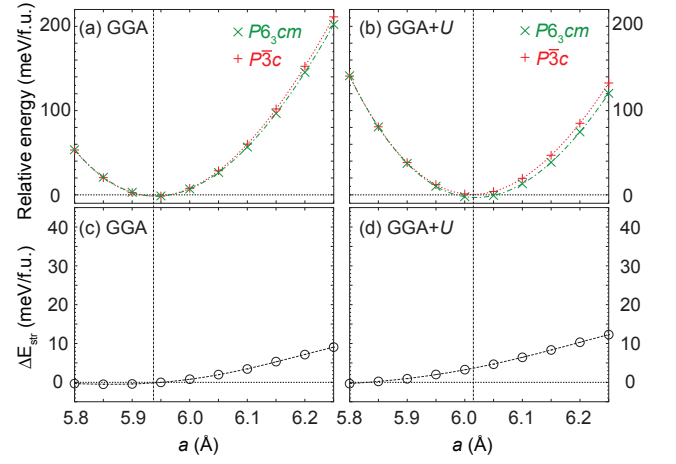


FIG. 9: (a),(b) Calculated InMnO_3 $P\bar{3}c$ and $P6_3cm$ structure energies relative to the equilibrium $P\bar{3}c$ phase as a function of in-plane lattice constant a by the GGA and GGA+U. (c),(d) Energy differences ΔE_{str} between the $P\bar{3}c$ and $P6_3cm$ phases. Positive values indicate that the ferroelectric $P6_3cm$ phase is stable over the $P\bar{3}c$ phase. The fitted lines were obtained with fourth-order polynomials. The vertical dashed lines indicate the calculated equilibrium lattice constants of InMnO_3 $P\bar{3}c$ phase.

sence of R -O hybridization is therefore a requirement for ferroelectricity in the hexagonal manganites. Earlier theoretical papers correctly noted the electrostatic origin of the “geometric ferroelectricity” mechanism in the hexagonal manganites;⁴ we now understand that the relative stability of ferroelectric and nonferroelectric structures is determined by a competition between electrostatics (favoring the ferroelectric phase) and covalency (favoring the nonferroelectric phase).

In addition, since the polar $P6_3cm$ and nonpolar $P\bar{3}c$ phases are close in energy in InMnO_3 as shown in Fig. 5, it might be expected that their relative stability could be changed using external perturbations such as epitaxial strain. Figure 9 shows the calculated energies of the $P6_3cm$ and $P\bar{3}c$ phases and their energy differences as a function of in-plane lattice constant a , with the out-of-plane lattice constant c and internal positions fully relaxed for each a value. Because the critical strain of the phase boundary depends on the U value, we performed the calculations using both the GGA and GGA+U methods. We see that the ΔE_{str} increases with the increasing in-plane lattice constant, indicating a larger in-plane lattice constant could develop the polar $P6_3cm$. Interestingly, the ferroelectric polarization develops in the out-of-plane direction, in striking contrast to the behavior in perovskites.³⁶ Therefore we anticipate that InMnO_3 could be tuned into the polar $P6_3cm$ structure using tensile strain.

Finally we mention that a recent transmission electron microscopy study of the domain walls in ferroelectric hexagonal TmMnO_3 and LuMnO_3 ³⁷ revealed that a domain wall structure at the edges of the sample is similar to the nonpolar $P\bar{3}c$ InMnO_3 structure: The R ion at the wall is at the centrosymmetric position, with one neighbor displaced in the up-direction and one in the down-direction. Detailed calculations

of the domain-wall structure in $RMnO_3$ are ongoing.

V. CONCLUSION

In summary, we have proposed a different nonferroelectric ground state structure in the hexagonal manganite $InMnO_3$, and we predict its occurrence in as-yet-unsynthesized hexagonal $TiMnO_3$. The proposed phase has $P\bar{3}c$ symmetry, and is closely related to the usual $P6_3cm$ ferroelectric ground state but with a different pattern of polyhedral tilts that retains the center of inversion. The energy balance between the two related phases is determined by a competition between electrostatics and R -O covalency, with *lower* R -O covalency favoring the ferroelectric structure. Thus, the *absence* of ferroelectricity in $InMnO_3$ reveals to us the reason for the *presence* of

ferroelectricity (and therefore multiferroicity) in the other h - $RMnO_3$ compounds.

Acknowledgments

We thank M. Bieringer, Department of Chemistry, University of Manitoba for providing the $InMnO_3$ single crystals. Y.K. acknowledges support by JSPS Postdoctoral Fellowships for Research Abroad. Y.K., M.L., N.L., M.F., and N.A.S. acknowledge support from ETH Zurich, and A.A.B. acknowledges support from MANA WPI Initiative (MEXT, Japan), FIRST Program (JSPS), and JSPS Grant No. 22246083. The SXRD was performed under Proposals No. 2009A1136 and No. 2010A1215. The visualization of crystal structures and charge density differences were performed with VESTA.³⁸

-
- * yu.kumagai@mat.ethz.ch
- ¹ T. Choi, Y. Horibe, H. Yi, Y. Choi, W. Wu, and S.-W. Cheong, *Nature Mater.* **9**, 253 (2010).
 - ² T. Jungk, A. Hoffmann, M. Fiebig, and E. Soergel, *Appl. Phys. Lett.* **97**, 012904 (2010).
 - ³ D. Meier, J. Seidel, A. Cano, K. Delaney, Y. Kumagai, M. Mostovoy, N. Spaldin, R. Ramesh, and M. Fiebig, *Nature Mater.* **11**, 284 (2012).
 - ⁴ B. Van Aken, T. Palstra, A. Filippetti, and N. Spaldin, *Nature Mater.* **3**, 164 (2004).
 - ⁵ C. J. Fennie and K. M. Rabe, *Phys. Rev. B* **72**, 100103 (2005).
 - ⁶ J. E. Greedan, M. Bieringer, J. F. Britten, D. M. Giaquinta, and H. C. zur Loye, *J. Solid State Chem.* **116**, 118 (1995).
 - ⁷ A. A. Belik, S. Kamba, M. Savinov, D. Nuzhnyy, M. Tachibana, E. Takayama-Muromachi, and V. Goian, *Phys. Rev. B* **79**, 054411 (2009).
 - ⁸ X. Fabrèges, I. Mirebeau, S. Petit, P. Bonville, and A. A. Belik, *Phys. Rev. B* **84**, 054455 (2011).
 - ⁹ D. A. Rusakov, A. A. Belik, S. Kamba, M. Savinov, D. Nuzhnyy, T. Kolodiaznyy, K. Yamaura, E. Takayama-Muromachi, F. Borodavka, and J. Kroupa, *Inorg. Chem.* **50**, 3559 (2011).
 - ¹⁰ C. R. Serrao, S. B. Krupanidhi, J. Bhattacharjee, U. V. Waghmare, A. K. Kundu, and C. N. R. Rao, *J. Appl. Phys.* **100**, 076104 (2006).
 - ¹¹ J. F. Scott, *J. Phys.: Condens. Matter* **20**, 021001 (2008).
 - ¹² E. Nishibori, M. Takata, K. Kato, M. Sakata, Y. Kubota, S. Aoyagi, Y. Kuroiwa, M. Yamakata, and N. M. Ikeda, *Nucl. Instrum. Methods Phys. Res. Sect. A* **467**, 1045 (2001).
 - ¹³ F. Izumi and T. Ikeda, *Mater. Sci. Forum* **198**, 321 (2000).
 - ¹⁴ The R values for nonpolar $P\bar{3}c$ are $R_{wp}=6.61\%$, $R_p=4.90\%$, $R_1=2.48\%$, and $R_F=1.39\%$. Those for polar $P6_3cm$ phase are $R_{wp}=6.64\%$, $R_p=4.94\%$, $R_1=2.36\%$, and $R_F=1.33\%$. Those for nonpolar $P6_3/mcm$ are $R_{wp}=12.94\%$, $R_p=8.90\%$, $R_1=6.08\%$, and $R_F=3.34\%$.
 - ¹⁵ H. L. Yakel, W. C. Koehler, E. F. Bertaut, and E. F. Forrat, *Acta Cryst.* **16**, 957 (1963).
 - ¹⁶ Although the $P\bar{3}c$ space group belongs to the trigonal group, in this study we use the term “hexagonal manganite” for simplicity to describe the structure class with $P\bar{3}c$ and $P6_3cm$ space groups for simplicity.
 - ¹⁷ R. D. King-Smith and D. Vanderbilt, *Phys. Rev. B* **47**, 1651 (1993).
 - ¹⁸ R. Birss, *Symmetry and Magnetism* (North-Holland, Amsterdam, 1966).
 - ¹⁹ M. Fiebig, V. Pavlov, and R. Pisarev, *J. Opt. Soc. Am. B* **22**, 96 (2005).
 - ²⁰ R. D. Shannon, *Acta Cryst.* **A32**, 751 (1976).
 - ²¹ P. E. Blöchl, *Phys. Rev. B* **50**, 17953 (1994).
 - ²² G. Kresse and J. Furthmüller, *Phys. Rev. B* **54**, 11169 (1996).
 - ²³ J. P. Perdew and A. Zunger, *Phys. Rev. B* **23**, 5048 (1981).
 - ²⁴ J. P. Perdew, K. Burke, and M. Ernzerhof, *Phys. Rev. Lett.* **78**, 1396 (1997).
 - ²⁵ S. L. Dudarev, G. A. Botton, S. Y. Savrasov, C. J. Humphreys, and A. P. Sutton, *Phys. Rev. B* **57**, 1505 (1998).
 - ²⁶ J. Medvedeva, O. Mryasov, M. Korotin, V. Anisimov, and A. Freeman, *J. Phys.: Condens. Matter* **12**, 4947 (2000).
 - ²⁷ M.-A. Oak, J.-H. Lee, H. M. Jang, J. S. Goh, H. J. Choi, and J. F. Scott, *Phys. Rev. Lett.* **106**, 047601 (2011).
 - ²⁸ We also performed calculations with the HSE06 hybrid functional (Ref. 39) that is known to describe the electronic structure for $3d$ transition metal compounds more precisely (Ref. 40–44). The calculated energy differences with FAFM configuration and $3\times 3\times 2$ k -points are 0.6 meV/f.u. for $InMnO_3$ and 19.9 meV/f.u. for $YMnO_3$, both of which are similar to the results in Fig. 5.
 - ²⁹ Y. Zhang and Y. Wang, *J. Electr. Mat.* **40**, 1501 (2011).
 - ³⁰ O. N. Mryasov and A. J. Freeman, *Phys. Rev. B* **64**, 233111 (2001).
 - ³¹ P. Ghosez, J.-P. Michenaud, and X. Gonze, *Phys. Rev. B* **58**, 6224 (1998).
 - ³² We calculated Z_R^* by displacing R cations in $P6_3/mmc$ in the z -direction. The obtained Z_R^* for $InMnO_3$ and $YMnO_3$ are $3.8|e|$ and $4.1|e|$. They are slightly higher than the formal charges, $3|e|$, but smaller than the Z^* s on d^0 cations in perovskites such as $BaTiO_3$ ($Z_{Ti}^* = 7.3|e|$) (Ref. 31).
 - ³³ D.-Y. Cho, J.-Y. Kim, B.-G. Park, K.-J. Rho, J.-H. Park, H.-J. Noh, B. Kim, S.-J. Oh, H.-M. Park, J.-S. Ahn, *et al.*, *Phys. Rev. Lett.* **98**, 217601 (2007).
 - ³⁴ M. Bieringer and J. Greedan, *J. Solid State Chem.* **143**, 132 (1999).
 - ³⁵ A. S. Gibbs, K. S. Knight, and P. Lightfoot, *Phys. Rev. B* **83**, 094111 (2011).
 - ³⁶ O. Diéguez, K. M. Rabe, and D. Vanderbilt, *Phys. Rev. B* **72**, 144101 (2005).
 - ³⁷ Q. H. Zhang, L. J. Wang, X. K. Wei, R. C. Yu, L. Gu, A. Hirata,

- M. W. Chen, C. Q. Jin, Y. Yao, Y. G. Wang, *et al.*, Phys. Rev. B **85**, 020102 (2012).
- ³⁸ K. Momma and F. Izumi, J. Appl. Cryst. **41**, 653 (2008).
- ³⁹ J. Heyd, G. E. Scuseria, and M. Ernzerhof, J. Chem. Phys. **124**, 219906 (2006).
- ⁴⁰ Y. Kumagai, Y. Soda, F. Oba, A. Seko, and I. Tanaka, Phys. Rev. B **85**, 033203 (2012).
- ⁴¹ H. Akamatsu, Y. Kumagai, F. Oba, K. Fujita, H. Murakami, K. Tanaka, and I. Tanaka, Phys. Rev. B **83**, 214421 (2011).
- ⁴² H. Akamatsu, K. Fujita, H. Hayashi, T. Kawamoto, Y. Kumagai, Y. Zong, K. Iwata, F. Oba, I. Tanaka, and K. Tanaka, Inorg. Chem. **51**, 4560 (2012).
- ⁴³ A. Stroppa, M. Marsman, G. Kresse, and S. Picozzi, New J. Phys. **12**, 093026 (2010).
- ⁴⁴ J. Hong, A. Stroppa, J. Íñiguez, S. Picozzi, and D. Vanderbilt, Phys. Rev. B **85**, 054417 (2012).